J|A|C|S ARTICLES

Published on Web 01/12/2009

Na_6ZnSn_2, $Na_{4.24}K_{1.76(1)}ZnSn_2$, and $Na_{20}Zn_8Sn_{11}$: Three Intermetallic Structures Containing the Linear $\{Sn-Zn-Sn\}^{6-}$ Unit

Sung-Jin Kim, Florian Kraus, and Thomas F. Fässler*

Department of Chemistry, Technische Universität München, Lichtenbergstrasse 4, D-85747 Garching, Germany

Received August 26, 2008; E-mail: thomas.faessler@lrz.tum.de

Abstract: The novel intermetallic compounds Na_6ZnSn_2 (**1**), $Na_{4.24}K_{1.76(1)}ZnSn_2$ (**2**), and $Na_{20}Zn_8Sn_{11}$ (**3**) were obtained from direct fusion of the pure elements, and their structures were determined by single crystal X-ray diffraction. All three compounds adopt new structure types and contain linear anionic $\{Sn-Zn-Sn\}^{6-}$ units with rather short Zn−Sn contacts (2.55−2.58 Å), separated by alkali metal counterions. Compound **3** comprises layers of interconnected heteroatomic $\{Zn_7Sn_5\}$ icosahedra as an additional unique structural motif. The bonding situation in this 16 valence-electron anion is analyzed by quantum chemical methods. The results of NBO, AIM, and ELF calculations (Gaussian03 on HF/3−21G level) reveal covalent bonding between Sn and Zn. The relationship to isovalent CO_2 is discussed. Band structure calculations on the density functional theory level (LMTO) show that **1** can be understood as a Zintl phase containing a $\{Sn-Zn-Sn\}^{6-}$ anion; however, Na−Sn contacts must also be considered. Magnetic susceptibility measurements show a temperature-independent, weak diamagnetism for Na_6ZnSn_2 (**1**).

1. Introduction

The class of polar intermetallic compounds shows a huge variety of different bonding patterns and new structures driven by the electronegativity differences between the involved electropositive and electronegative metals and semimetals. In the case of Zintl phases[1] the bonding of the anionic substructures can be explained by electron counting rules, such as the $(8-N)$ rule. These concepts also include the description of electron-deficient compounds and systems with multiple and delocalized bonds by applying Wade's rules[2] for polyhedral building blocks.[3] Recently the family of $s-p$ bonded binary Zintl compounds A/E (A = alkali or alkaline earth metal; E = main group metal) has been further extended to ternary systems A/M/E with transition metals M, e.g., Ti,[4] Mn,[5] Au,[6] or group 12 metals Zn,[7] Cd,[8] and Hg.[9] In many cases the connectivity of the atoms of the anionic part of the structures can be tuned by the sheer amount of electrons provided by the electropositive metal. Electron-poorer phases exhibit structures of atoms or clusters that are arranged in networks, whereas electron-richer phases often contain isolated anions without further bonding to other atoms but with higher formal charges.

Triatomic linear units with sixteen valence electrons (VE) isovalent to CO_2 or $HgCl_2$ in intermetallic compounds are of special interest, since such units may show multiple bonding and have counterparts in molecules and salts. The majority of representatives is found among the ternary alkali metal/beryllium- and alkali metal/boron-pnictides, such as K_4BePn_2 (Pn = P, As, Sb),[10] A_3BP_2, A_3BAs_2 (A = K),[11] A_3BP_2, (A = Na, Na/K, Rb, Cs), A_3BAs_2 (A = Rb, Cs),[12] or in combination with group 11 and 12 elements, e.g., Na_4HgP_2, K_4MP_2 (M = Zn, Cd, Hg),[13] K_5AuPn_2 (Pn = P, As), K_5CuPn_2 (Pn = As, Sb),[14,15] and K_4ZnAs_2.[16] Furthermore, nitridoborate $\{BN_2\}^{3-}$,[17−19] cyanamide (carbodiimide) $\{CN_2\}^{2-}$,[20] and carbidoborate $\{BC_2\}^{5-}$[21] units exist, which have also been found in some double salts,

(1) Zintl, E.; Gobeau, J.; Dullenkopf, W. *J. Phys. Chem.* **1931**, *A 154*, 1.
(2) Wade, K. *Adv. Inorg. Chem. Radiochem.* **1976**, *18*, 1.
(3) Nesper, R. *Angew. Chem., Int. Ed.* **1991**, *30*, 789.
(4) (a) Stuhrmann, J.; Adam, A.; Schuster, H. U. *Z. Naturforsch.* **1993**, *48*, 898. (b) Nuss, J.; Hoenle, W.; Peters, K.; von Schnering, H. G. *Z. Anorg. Allg. Chem.* **1996**, *622*, 1879.
(5) (a) Rehr, A.; Kuromoto, T. Y.; Kauzlarich, S. M.; del Castillo, J.; Webb, D. J. *Chem. Mater.* **1994**, *6*, 93. (b) Park, S. M.; Kim, S. J.; Kanatzidis, M. G. *Inorg. Chem.* **2005**, *44*, 4979.
(6) (a) Li, B.; Corbett, J. D. *Inorg. Chem.* **2005**, *44*, 6515. (b) Li, B.; Corbett, J. D. *Inorg. Chem.* **2006**, *45*, 8958. (c) Li, B.; Corbett, J. D. *J. Am. Chem. Soc.* **2006**, *128*, 12392.
(7) (a) Queneau, V.; Sevov, S. C. *J. Am. Chem. Soc.* **1997**, *119*, 8109. (b) Kim, S.-J.; Hoffmann, S. D.; Fässler, T. F. *Angew. Chem., Int. Ed.* **2007**, *46*, 3144.
(8) (a) Todorov, E.; Sevov, S. C. *Angew. Chem., Int. Ed.* **1999**, *38*, 1775. (b) Xia, S.; Bobev, S. *J. Am. Chem. Soc.* **2007**, *129*, 4049.
(9) Kaltzoglou, A.; Ponou, S.; Fässler, T. F. *Eur. J. Inorg. Chem.* **2008**, 538.
(10) Somer, M.; Hartweg, M.; Peters, K.; Popp, T.; von Schnering, H. G. *Z. Anorg. Allg. Chem.* **1991**, *595*, 217.
(11) von Schnering, H. G.; Somer, M.; Hartweg, M.; Peters, K. *Angew. Chem.* **1990**, *102*, 63.
(12) Somer, M.; Carillo-Cabrera, W.; Peters, K.; von Schnering, H. G. *Z. Anorg. Allg. Chem.* **2000**, *626*, 897.
(13) (a) Eisenmann, B.; Somer, M. *Z. Naturforsch.* **1985**, *40 B*, 1419. (b) *Z. Naturforsch.* **1989**, *44 B*, 1228.
(14) Eisenmann, B.; Klein, J.; Somer, M. *J. Alloys Compd.* **1992**, *178*, 431.
(15) Savelsberg, G.; Schäfer, H. *Z. Naturforsch.* **1979**, *34 B*, 771.
(16) Prots, Y.; Aydemir, U.; Öztürk, S. S.; Somer, M. *Z. Kristallogr. NCS* **2007**, *222*, 163.
(17) Goubeau, J.; Anselment, W. *Z. Anorg. Allg. Chem.* **1961**, *310*, 248.
(18) Häberlen, M.; Glaser, J.; Meyer, H. J. *J. Solid State Chem.* **2005**, *178*, 1478.
(19) Wörle, M.; Meyer zu Altenschildesche, H.; Nesper, R. *J. Alloys Compd.* **1998**, *264*, 107.
(20) Vannerberg, N. G. *Acta Chem. Scand.* **1962**, *16*, 2263.
(21) Reckeweg, O.; Meyer, H. J. *Angew. Chem.* **1998**, *110*, 3619.

and the most prominent representatives in molecular chemistry, i.e., $\{NO_2\}^+$, $\{N_3\}^-$, $\{C_3\}^{4-}$, $\{CS_2\}$, and $\{NS_2\}^+$, have been reviewed.[22]

The notably short interatomic distances in such discrete polyanions bring up the question about the nature of their chemical bonding. In the case of $\{BPn_2\}^{3-}$ (Pn = P, As) a cumulene-like system was concluded from both X-ray and vibrational measurements.[11] Bond-stretch isomerism was reported for $\{CN_2\}^{2-}$,[23] and in most cases the interatomic distances are in the range typical of multiple bonding, and significant $(p-p)\pi$ bonding must be taken into account. Comparison of the structures and properties of molecules or anions with those of analogous moieties in intermetallic compounds is a suggestive approach to probe classical bonding principles in intermetallics. Although further theoretical studies could shed more light on the nature of the chemical bonding (especially interesting in the presence of the heavier carbon homologues Ge or Sn) theoretical analyses and investigations of the electronic structure of 16 VE triatomic linear monomers in intermetallic compounds have not been reported so far.

In this context we focus on the ternary sodium zinc stannides that have not been thoroughly explored yet. Investigation of ternary systems including Na, Zn, and Sn show the validity of the pseudoelement approach: Systems with elements of rather similar electronegativity (Zn and Sn) and an average number of valence electrons corresponding to that of a main group element are expected to adopt structures similar to that of the respective p-block element (Ga). In fact our exploratory studies of such intermetallic phases led to Ga analogous cluster compounds on the Na-poor side,[7b] whereas on the alkali metal rich side of the phase diagram the title compounds **1**−**3** were obtained. Herein we report the syntheses and structures of the three new phases Na_6ZnSn_2 (**1**), $Na_{4.24}K_{1.76(1)}ZnSn_2$ (**2**), and $Na_{20}Zn_8Sn_{11}$ (**3**). It is interesting to note that the $\{ZnSn_2\}^{6-}$ units in **1**−**3** remain almost unchanged upon K for Na substitution. Together with the structurally related $\{CuSb_2\}^{5-}$[15] unit, these $\{ZnSn_2\}^{6-}$ moieties of the title compounds are good candidates for a detailed investigation of the chemical bonding based on quantum chemical methods.

2. Experimental Section

2.1. Synthesis. The title compounds Na_6ZnSn_2 (**1**), $Na_{4.24}K_{1.76(1)}ZnSn_2$ (**2**), and $Na_{20}Zn_8Sn_{11}$ (**3**) were prepared by direct fusion of the pure elements (Na: rods, Merck; Zn: freshly distilled, Merck, Sn: drops 99.95%, Aldrich) in tantalum ampoules. Manipulations of all chemicals took place in an Ar-filled glovebox (O_2 and H_2O levels <0.1 ppm). The loading ratios used were Na/K/Zn/Sn = 6:0:0.9:2 for **1**, 3:2:1:2 for **2**, and 20:0:8:11 for **3**. After filling, the ampoules were sealed and placed into fused silica tubes, which were evacuated and afterward heated to 773 K at a rate of 2 $K\cdot min^{-1}$. Homogenization at that temperature for 10 h was followed by slow cooling (0.1 $K\cdot min^{-1}$) to room temperature and yielded highly air-sensitive dark crystalline products which contained the title compounds. Phase analysis of the products was done by X-ray powder diffraction using an STOE STADI P2 diffractometer (Ge(111) monochromator for Cu $K\alpha_1$ radiation: λ = 1.540 56 Å) equipped with a linear position-sensitive detector. The sample preparation was performed in a glovebox: the reaction product was finely ground in an agate mortar, diluted with diamond powder, and filled into a glass capillary which then was sealed using a red-hot tungsten wire. All samples were measured in Debye−Scherrer mode ($2\theta_{max}$ = 80°), and the data analysis was done using the STOE WinXPOW software package. The phases were identified by comparing experimental and calculated powder patterns from the single crystal refinements. According to the X-ray powder diagrams the compounds were obtained in high yields (>80%), and main admixtures were $Na_{15}Sn_4$[25] and $NaZn_{13}$[26] for **1** and β-NaSn[27] and $NaZn_{13}$ for **3**, and for the quaternary phase **2** several weak reflections were detected that could not be assigned to known compounds. All side products were obtained essentially as microcrystalline powders, whereas the target compounds were received as large single crystals. Although K-poorer phases, such as $Na_{5.57}K_{0.43(1)}ZnSn_2$, are accessible, the pure K analogue of **1** could not be obtained yet. Corresponding experiments yielded products with a higher content of amorphous byproducts accompanied by K_6Sn_{25}[28] and KSn[29] as the only crystalline phases. Compound **2** marks the K-richest phase (lower K loadings resulted in K-poorer single crystals, as mentioned above).

2.2. Elemental Analysis. Semiquantitative standardless EDX analysis was performed with a JEOL 5900LV scanning electron microscope which was equipped with a Röntec EDX detector and operated at 20 kV accelerating voltage. Inside the glovebox several crystallites from each compound were fixed with carbon tape onto an aluminum sample holder. During the transfer of the samples into the microscope chamber, they were shortly exposed to air. Thus, images from secondary electrons revealed partial surface oxidation, but enough smooth areas were available for the measurements. Analysis of three spots per crystallite with a counting time of 3 min for each spot showed average atomic Na/K/Zn/Sn compositions (%) of 70(6):0:8(2):22(2) for **1**, 51(4):16(3):9(2):24(3) for **2**, and 55(4):0:17(3):28(2) for **3**. Despite the large standard deviations of the measurements, these results confirm the presence of the elements and are roughly in agreement with the compositions obtained from single crystal X-ray studies (the calculated values Na/K/Zn/Sn are 67:0:11:22 for **1**, 47:20:11:22 for **2**, and 51:0:21:28 for compound **3**).

2.3. Single Crystal X-ray Structure Studies. Single crystals were selected in an Ar-filled glovebox and sealed into glass capillaries. X-ray diffraction data were collected on an Oxford Xcalibur3 diffractometer with graphite-monochromated Mo Kα radiation (λ = 0.710 73 Å) at 293 K. The measurements comprised four sets of ω scans (and an additional φ scan for **2**) with acquisition rates of 20 s/frame and a scan width of 1°. The data were corrected for absorption (empirical, ABSPACK):[30] The structures of **1**, **2**, and **3** were solved by Direct Methods and refined anisotropically in the monoclinic space groups *C*2/*m*, $P2_1/c$, and *C*2/*c*, respectively, using SHELXTL.[31] Details of the X-ray data collection and structural refinements are listed in Table 1. Final equivalent isotropic displacement parameters and selected interatomic distances are listed in Tables S1−S3 (Supporting Information, together with further details of the refinements). For Na_6ZnSn_2 (**1**) the indexing routine indicated a centered monoclinic lattice, and no additional systematic extinctions were observed, leading to *C*2, *Cm*, and *C*2/*m* as the possible space groups. Solutions in rhombohedral[32] and the lower-symmetric monoclinic space groups did not lead to a significant improvement, and therefore the higher-symmetric one (*C*2/*m*, No.

(22) Klapötke, T. M. *Angew. Chem., Int. Ed.* **1994**, *33*, 1575.
(23) Liu, X.; Müller, P.; Kroll, P.; Dronskowski, R. *Inorg. Chem.* **2002**, *41*, 4259.
(24) Rodriguez-Carvajal, R. *Physica B* **1993**, *192*, 55.
(25) Mueller, W.; Volk, K. *Z. Naturforsch.* **1978**, *33 B*, 275.
(26) Zintl, E.; Haucke, W. *Z. Elektrochem.* **1938**, *44*, 104.
(27) Mueller, W.; Volk, K. *Z. Naturforsch.* **1977**, *32 B*, 709.
(28) Fässler, T. F.; Kronseder, C. *Z. Anorg. Allg. Chem.* **1998**, *624*, 561.
(29) Hewaidy, I. F.; Busmann, E.; Klemm, W. *Z. Anorg. Allg. Chem.* **1964**, *328*, 283.
(30) Scale3/ABSPACK, *CrysAlis RED, Oxford Diffraction Ltd., Version 1.171.32* 2007.
(31) (a) Sheldrick, G. *SHELXS-97, Program for the Solution of Crystal Structures*, Universität Göttingen 1997. (b) Sheldrick, G. *SHELXL-97, Program for the Refinement of Crystal Structures*, Universität Göttingen 1997. (c) SHELXTL, *Bruker Analytical X-ray instruments*: Madison, WI 1998.
(32) The related structure of K_4CdP_2 formerly described in space group $C2/m$[13a] was revised later in $R\bar{3}m$.[13b]

Table 1. Crystallographic Data for $Na_{6-x}K_xZnSn_2$ ($x = 0$ (**1**), 1.76(1) (**2**)) and $Na_{20}Zn_8Sn_{11}$(**3**)

empirical formula	Na_6ZnSn_2(1)	$Na_{4.24}K_{1.76(1)}ZnSn_2$(2)	$Na_{20}Zn_8Sn_{11}$(3)
formula weight/g·mol^{-1}	440.69	469.12	2288.35
temperature/K		293(2)	
diffractometer		Oxford Xcalibur3 (CCD)	
crystal system		monoclinic	
space group	*C*2/*m* (No. 12)	$P2_1/c$ (No. 14)	*C*2/*c* (No. 15)
color of crystal	black	black	silvery
unit cell parameters/Å	$a = 10.077(3)$	$a = 11.572(1)$	$a = 16.151(1)$;
	$b = 5.473(1)$	$b = 9.862(1)$	$b = 9.276(1)$;
	$c = 9.316(2)$	$c = 11.382(1)$	$c = 27.594(2)$
	$\beta = 98.07(2)°$	$\beta = 119.33(1)°$	$\beta = 102.97(1)°$
unit cell volume/Å^3; Z	508.7(1); 2	1132.3(1); 4	4028.6(5); 4
goodness of fit on F^2	0.928	0.986	1.222
R_1/wR_2 [$I \geq 2\sigma(I)$]	0.022/0.044	0.029/0.062	0.035/0.078
R_1/wR_2 (all data)	0.032/0.045	0.045/0.067	0.041/0.087

12, Pearson code *mC*18) was chosen for the refinement. During structure solution and refinement three Na, one Sn, and one Zn sites could be assigned. The final refinement has an R_1 value (all data) of 0.032 and a featureless residual map. The structure of $Na_{4.24}K_{1.76(1)}ZnSn_2$ (**2**) was solved in the centrosymmetric space group $P2_1/c$ (No. 14, Pearson code *mP*40). Two Sn, one Zn, and six alkali metal positions could be assigned. After refinement, two of the positions assigned to Na showed significantly smaller atomic displacement parameters, and further refinement converged significantly when one of these positions was assigned to K (full occupation, K2) and the other one to Na and K (A) with site occupancy 0.23/0.77. The structure of $Na_{20}Zn_8Sn_{11}$ (**3**) was solved in the monoclinic space group *C*2/*c* (No. 15, Pearson code *mC*156). Upon anisotropic refinement we assigned six Sn, four Zn, and 10 Na positions. Sn5 showed slightly enlarged displacement values and was therefore refined as mixed-occupied with Zn (49.3%, fixed to 50.0% during the final refinement cycles). Zn4 which is located on a center of inversion (Wyckoff site 4*d*) showed an elongated anisotropic displacement parameter (ADP) along *a*, and the adjacent sodium atoms (Na10) also displayed a large anisotropy. A splitting of this site and twin refinement did not result in a significant improvement of the structure model, and lowering of the symmetry to subgroups, such as *Cc* (No. 9), *C*2 (No. 5), or $C\bar{1}$ (No. 2), led to comparable results. Partial data collection using an X-ray beam with higher intensity (rotating anode: Bruker Nonius FR591 and STOE IPDS 2T diffractometer) at room and low temperature (100 K) showed strong diffuse scattering along *c**. As no satellite reflections could be detected this feature correlates with poor atomic ordering in the layers associated with the Zn4 and Na10 positions (*ab* plane) leading to larger ADPs.

2.4. Electronic Structure Calculations. 2.4.1. LMTO Calculations. The electronic structure of Na_6ZnSn_2 (**1**) was calculated with the local density-functional approach and the linear muffin-tin orbital (LMTO) method in the atomic sphere approximation (ASA) using the tight-binding (TB) program LMTO47c.[33] The radii of the muffin-tin spheres and empty spheres were determined after Jepsen and Andersen.[34−36] The *k*-space integration was performed by the tetrahedron method on a set of 554 irreducible *k* points and a basis set with Na-3*s*/(3*p*)/(3*d*), Zn-4*s*/4*p*/3*d*, Sn-5*s*/5*p*/(5*d*)/(4*f*) (down-folded orbitals in parentheses). The crystal orbital Hamilton population (COHP)[37] method was used for the analysis of bonding interactions and is analogous to the crystal orbital overlap population (COOP) method used in the semiempirical Hückel calculations. The Fermi level in all figures is set to zero, and the COHP diagrams are drawn by reversing their values with respect to the energy scale (i.e., −COHP vs *E*). By this the calculated peak values become negative for antibonding and positive for bonding interactions.

2.4.2. NBO (Natural Bond Orbital Analysis), AIM (Atoms in Molecules), and ELF (Electron Localization Function) Analysis. *Ab initio* calculations were carried out for the isolated unit $\{ZnSn_2\}^{6-}$ as obtained from the crystal structure of Na_6ZnSn_2 (**1**) using Gaussian03[38] with the TOPMOD[39] program package at HF/3−21G levels of theory.[40] For comparison the calculations were performed for $\{Na_{20}ZnSn_2\}^{14+}$ and for an acetonitrile-solvated polarizable continuum model (PCM) unit denoted with the indices "Na20" and "solv", respectively. Molecular orbital diagrams and ELF[41] diagrams were obtained with GaussView[42] and MOLEKEL[43] programs.

2.5. Magnetic Measurements. Magnetic susceptibility measurements for Na_6ZnSn_2 (**1**) were performed with an MPMS XL SQUID Magnetometer (Quantum Design). Single crystals from different batches were measured to ensure reproducibility. Several crystals were manually collected, and the cell constants of some of them were checked. All met the metric of crystals of compound **1**. 20.9 mg of the substance were closed in a gelatine capsule which was fixed in a plastic straw. At a 20 G field cooling and heating measurements were performed from 2 to 300 K. The obtained data indicate a temperature-independent weak diamagnetism for Na_6ZnSn_2. A graphical representation of $\chi(T)$ is shown in Figure S4 (Supporting Information).

3. Results and Discussions

3.1. Structure Descriptions. Na_6ZnSn_2 (**1**), $Na_{4.24}K_{1.76(1)}ZnSn_2$ (**2**), and $Na_{20}Zn_8Sn_{11}$ (**3**) represent new intermetallic phases which all contain isolated $\{ZnSn_2\}^{6-}$ units. **3** comprises layers of interconnected heteroatomic $\{Zn_7Sn_5\}$ icosahedra as an additional unique structural motif.

3.1.1. Na_6ZnSn_2 (1). The unit cell of **1**, as shown in Figure 1a, features isolated linear units of $\{Sn-Zn-Sn\}^{6-}$ anions with an intramolecular Zn−Sn distance of 2.561(1) Å. These anions are oriented parallel to each other (roughly along [102]) and are well separated by the Na counterions (nearest intermolecular Sn−Sn or Zn−Zn contacts are >5.4 Å). The anionic rods are embedded into $\{Na_{20}\}$ polyhedra with Na−Sn, Na−Zn, and Na−Na contacts up to 3.8 Å (Figure 1c and 3a).[44] Additionally, Na1 and Na3 form a layer of distorted $\{(Na3)_6(Na1)_2\}$ cubes in the *ab* plane, as depicted in Figure 1b. The Na−Na distances within these cubes range from 3.414(2) to 3.667(5) Å and are only slightly shorter (3.67 Å) than in elemental *bcc*-Na. These cubes efficiently fill voids and separate the layers of condensed $\{Na_{20}\}$ polyhedra.

As shown in the bottom part of Figure 1a, the structure can also be described by hexagonal double layers of Sn atoms in analogy to an *fcc* lattice with the Sn−Zn−Sn units representing two edges of the resulting distorted Sn octahedra and the Na

(33) Tank, R. W.; Jepsen, O.; Burkhardt, A.; Andersen, O. K. *TB-LMTO-ASA 4.7*; Max-Planck-Institut für Festkörperforschung, Stuttgart, Germany 1998.
(34) Jepsen, O.; Andersen, O. K. *Z. Phys. B* **1995**, *97*, 35.
(35) Blöchl, P. E.; Jepsen, O.; Andersen, O. K. *Phys. Rev. B* **1994**, *49*, 16223.
(36) Andersen, O. K.; Jepsen, O. *Phys. Rev. Lett.* **1984**, *53*, 2571.
(37) Blöchl, P. E.; Dronskowski, R. *J. Phys. Chem.* **1993**, *97*, 8617.
(38) Frisch, M. J. et al. *Gaussian 03, Revision D.01*, Gaussian, Inc., Wallingford CT, 2004.
(39) Noury, S.; Krokidis, X.; Fuster, F.; Silvi, B. *Computers & Chemistry* **1999**, *23*, 597.
(40) Schuchardt, K. L.; Didier, T.; Elsethagen, T.; Sun, L.; Gurumoorthi, V.; Chase, J.; Li, J.; Windus, T. L. *J. Chem. Inf. Model* **2007**, *47*, 1045.
(41) Becke, A. D.; Edgecombe, K. E. *J. Chem. Phys.* **1990**, *92*, 5397.
(42) GaussView, Dennington, R.; Keith, T.; Millam, J.; Eppinnett, K.; Hovell, W. L.; Gilliland, R. Semicham Inc., Shawnee Mission, KS 2003.
(43) Flükiger, P.; Lüthi, H. P.; Portman, S.; Weber, J. *Molekel 4.0*; Manno (Switzerland), Swiss Center for Scientific Computing, 2000.
(44) Similar $\{A_{14}\}$ and $\{A_{14+3}\}$ cages were found in K_5CuSb_2[15] and K_5CuAs_2,[14] respectively.

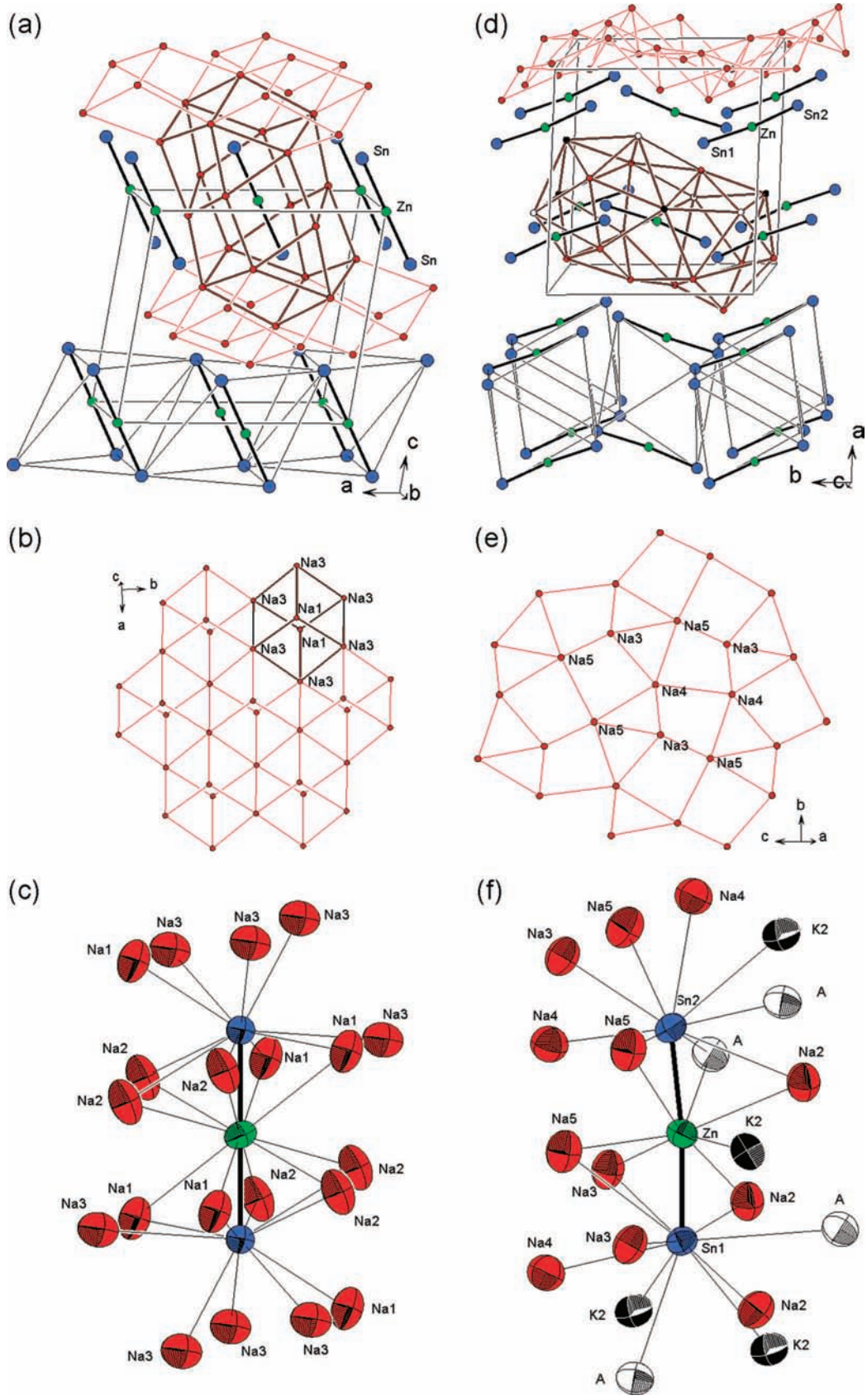

Figure 1. Structural details of Na_6ZnSn_2 (a−c) (**1**) and $Na_6K_{4.24}Zn_{1.76(1)}Sn_2$ (d−f) (**2**): (a) View of the structure along [010]. A $\{Na_{20}\}$ polyhedron is emphasized with thick red, $\{ZnSn_2\}$ units with thick black, distorted cubes of Na atoms with thin red, and tin octahedra by thin black lines. (b) A layer of distorted Na cubes made of Na1 and Na3 atoms; one cube is emphasized. (c) Arrangement of the Na atoms around the $\{ZnSn_2\}$ triatomic unit for interatomic distances up to 4 Å (atoms are drawn at 70% probability level). (d) View of the structure along [001]. (e) Single puckered layer made of Na3, Na4, and Na5 atoms. (f) Arrangement of the alkali atoms around the $\{ZnSn_2\}$ unit for interatomic distances up to 4 Å (thermal ellipsoids at 70% probability level). Na, K, A = Na/K, Sn, and Zn atoms are represented as red, black, empty, blue, and green spheres, respectively.

atoms being distributed within the resulting voids (for an additional illustration, see the Supporting Information).

As expected, the slightly more electropositive Zn atom is located in the center of the linear {Sn−Zn−Sn} unit which is in agreement with the site preference in three-center species.[45] The Zn−Sn distance (2.56 Å) is comparable to Zn−Sn separations found in $Ca_{4.66}Sn_3Zn_{0.7}$[46] (2.49 Å) and is considerably shorter as compared to the ones found in $BaZn_2Sn_2$[47] (2.79 Å), $Na_{29}Zn_{24}Sn_{32}$ (2.72 Å),[7b] BaZnSn (2.71 Å),[48] or GdZnSn (2.68 Å),[49] and also shorter as the sum of Pauling's covalent radii of 2.65 Å (r(Sn) = 1.40 Å, r(Zn) = 1.25 Å).[50,51] However, in the above examples the valence angle at the Zn atom shows significant deviations from linearity, and the triatomic units are not discrete. In **1** the average Na−Zn and Na−Sn distances within the confining Na cage (Figure 1c) are 3.49 and 3.36 Å, respectively. The slight preference of Na toward Sn can be explained by the higher electronegativity of Sn as compared to that of Zn (Pauling scale[51,52]).

3.1.2. $Na_{4.24}K_{1.76(1)}ZnSn_2$ (2). A slightly bent {Sn−Zn−Sn}$^{6-}$ unit with a Sn−Zn−Sn bond angle of 172.26(1)° and two different Zn−Sn distances (d(Sn1−Zn) = 2.582(1), d(Sn2−Zn) = 2.556(1) Å) are found in the structure of **2**. The unit cell (Figure 1d) shows well isolated anions with interunit Sn−Sn and Sn−Zn distances larger than 5 Å. The anions are embedded into {A_{20}} polyhedra (12 × Na, 4 × K, 4 × A, Figure 3b). The corrugated ($3^2.4^2$)($3.4.3.4^2$)($3^2.4^3$) nets[53] of Na3 to Na5 atoms form the interface between the {A_{20}} polyhedra (Figure 1d and 1e).

As in compound **1** the atom packing can also be described on the basis of distorted octahedra with two {Sn−Zn−Sn} units forming the basal plane and Sn atoms of adjacent units serving as apex atoms (Figure 1d). The distorted octahedra share vertices and form layers in the *bc* plane which are primitively stacked along *a* and are separated by Na atoms (for an additional illustration see the Supporting Information). Again high coordination numbers of the Zn and Sn atoms are detected. The Zn atom is surrounded by seven, and the Sn atoms are coordinated by 9 to 10 alkali metal atoms with a distance range from 3.07 to 3.98 Å (Figure 1f). The two different Sn−Zn bond lengths might originate from the different environment. Whereas the Sn1−Zn bond is bridged by two Na atoms, a further A = Na/K bridge exists in the case of the shorter Sn2−Zn bond. Due to the large differences of the ionic radii and the Pauling electronegativity of Na and K compounds **1** and **2** are not isopointal. Related structural changes have also been observed in the systems ASi and AGe (A = Na, K) containing tetrahedral polyanions.[54]

3.1.3. $Na_{20}Zn_8Sn_{11}$ (3). $Na_{20}Zn_8Sn_{11}$ represents a new structure type. It can be described as an alternate stacking of a layer of icosahedral {Zn_7Sn_5} clusters, which are connected by Sn1 atoms, and a layer containing {$ZnSn_2$} units similar to those found in compounds **1** and **2** (Figure 2a). The triatomic unit features a central Zn4 and two terminal Sn5 atoms at a short distance of 2.546(1) Å. This unit is surrounded by 18 Na atoms at distances shorter than 4 Å. The {Zn_7Sn_5} icosahedron with its center at the (4*e*)-site contains three different Zn atoms (Zn1 to Zn3), two Sn atoms (Sn2, 3), and one mixed-occupied M atom (Sn and Zn with equal ratio) (Figure 2c). All possible homo- and heteroatomic contacts are present and range from 2.763(1) to 2.959(1) Å. The values are in the range of the sum of Pauling's covalent radii for Zn and Sn and comparable to distances found, e.g., in $Na_{29}Zn_{24}Sn_{32}$.[7b] Within the *ab* plane each icosahedron forms six *exo*-bonds *via* four of its Zn and two M atoms to Sn1 atoms (Figure 2b). Sn1 adopts a flat trigonal pyramidal coordination with valence angles between 112.6° and 117.1°[55] and connects three icosahedra in alternating orientations.[57] The two Zn1 vertices display additional *exo*-bonds to Sn4 atoms at a distance of 2.687(1) Å. All *exo*-cluster contacts are slightly shorter than the corresponding intracluster distances (Table S3). The remaining cluster atoms Sn2 and Sn3 show no further *exo*-contacts.

Typically, icosahedra are formed in compounds with a higher degree of electron deficiency as in many phases of the triele elements in which icosahedra are interconnected through all vertices.[6,59] In the structure of **3** the polyhedra however exhibit only eight *exo*-bonds. The *exo*-bonds in **3** are exclusively established *via* Zn and M and not *via* Sn atoms. This might be explained by lone pair formation at the Sn vertex atoms. The existence of lone pairs at the vertices of polyhedra has been well established for the class of homoatomic Zintl ions such as {Sn_n}$^{4-}$ (n = 4, 9). The polyhedra in $Na_{20}Zn_8Sn_{11}$ can therefore be regarded as more electron-rich, which explains their coexistence with highly charged linear anionic units.

The icosahedra in **3** are surrounded by {Na_{20}} pentagonal dodecahedra (pdod). The latter share edges and form layers of polyhedra in the *ab* plane. In the [001] direction each layer is separated by layers of {Na_{18}} cages which surround the {$ZnSn_2$} units (Figure 3c).

3.2. Electron and Bonding Requirements. **1** and **2** are Zintl phases assuming a complete electron transfer from the alkali metal atoms to Sn and Zn atoms. The charge distribution in the resulting {$ZnSn_2$}$^{6-}$ anion can be rationalized in various ways, as outlined in Scheme 1. Formula **I** represents a fully ionic description, whereas in **II** two Sn atoms are covalently bound to the central Zn atom and **III** assumes multiple bonding between the Zn and Sn atoms. The calculation of bond orders according to Pauling (PBO)[50] results in values of 1.4 and 1.3 for **1** and **2**, respectively. Further, the calculated Zn−Sn bond lengths (2.56−2.58 Å) are shorter than those reported for molecular compounds, such as [MeSi{Si-Me_2N(*p*-Tol)}$_3$Sn]$_2$Zn[60] and Zn[bis[3-(dimethylamino)propyl-C,N]Sn-

(45) Burdett, J.; Lawrence, N. J.; Turner, J. J. *Inorg. Chem.* **1984**, *23*, 2419.
(46) Ganguli, A. K.; Gupta, S.; Zhao, J. T.; Leon-Escamilla, E. A.; Corbett, J. D. *J. Solid State Chem.* **2005**, *178*, 2959.
(47) Eisenmann, B.; May, N.; Müller, W.; Schäfer, H. *Z. Naturforsch.* **1972**, *27*, 1155.
(48) Merlo, F.; Fornasini, M. L.; Pani, M. *J. Less-Comm. Met.* **1991**, *171*, 329.
(49) Manfrinetti, P.; Pani, M. *J. Alloys Compd.* **2005**, *393*, 180.
(50) Pauling, L. *J. Am. Chem. Soc.* **1947**, *69*, 542.
(51) Pauling, L. *Die Natur der chemischen Bindung*; Verlag Chemie: Weinheim 1968.
(52) Pauling, L. *J. Am. Chem. Soc.* **1932**, *54*, 3570.
(53) Schläfli symbols denote types and numbers of polygons around the net points.
(54) (a) Witte, J.; von Schnering, H. G. *Z. Anorg. Allg. Chem.* **1964**, *327*, 260. (b) Busmann, E. *Z. Anorg. Allg. Chem.* **1961**, *313*, 90.
(55) A similar coordination of Sn atoms is found in triphenyltin substituted molecules.[56]
(56) Englich, U.; Ruhland-Senge, K.; Uhlig, F. *J. Organomet. Chem.* **2000**, *613*, 139.
(57) A similar array of icosahedra is found in MgB_9N.[58]
(58) Mironov, A.; Kazakov, S. M.; Jun, J.; Karpinski, J. *Acta Crystallogr., Sect. C* **2002**, *58*, i95.
(59) Tillard-Charbonnel, M.; Manteghetti, A.; Belin, C. *Inorg. Chem.* **2000**, *39*, 1684, and references therein.
(60) Lutz, M.; Findeis, B.; Haukka, M.; Graff, R.; Pakkanen, T. A.; Gade, L. H. *Chem. Eur. J.* **2002**, *8*, 3269.

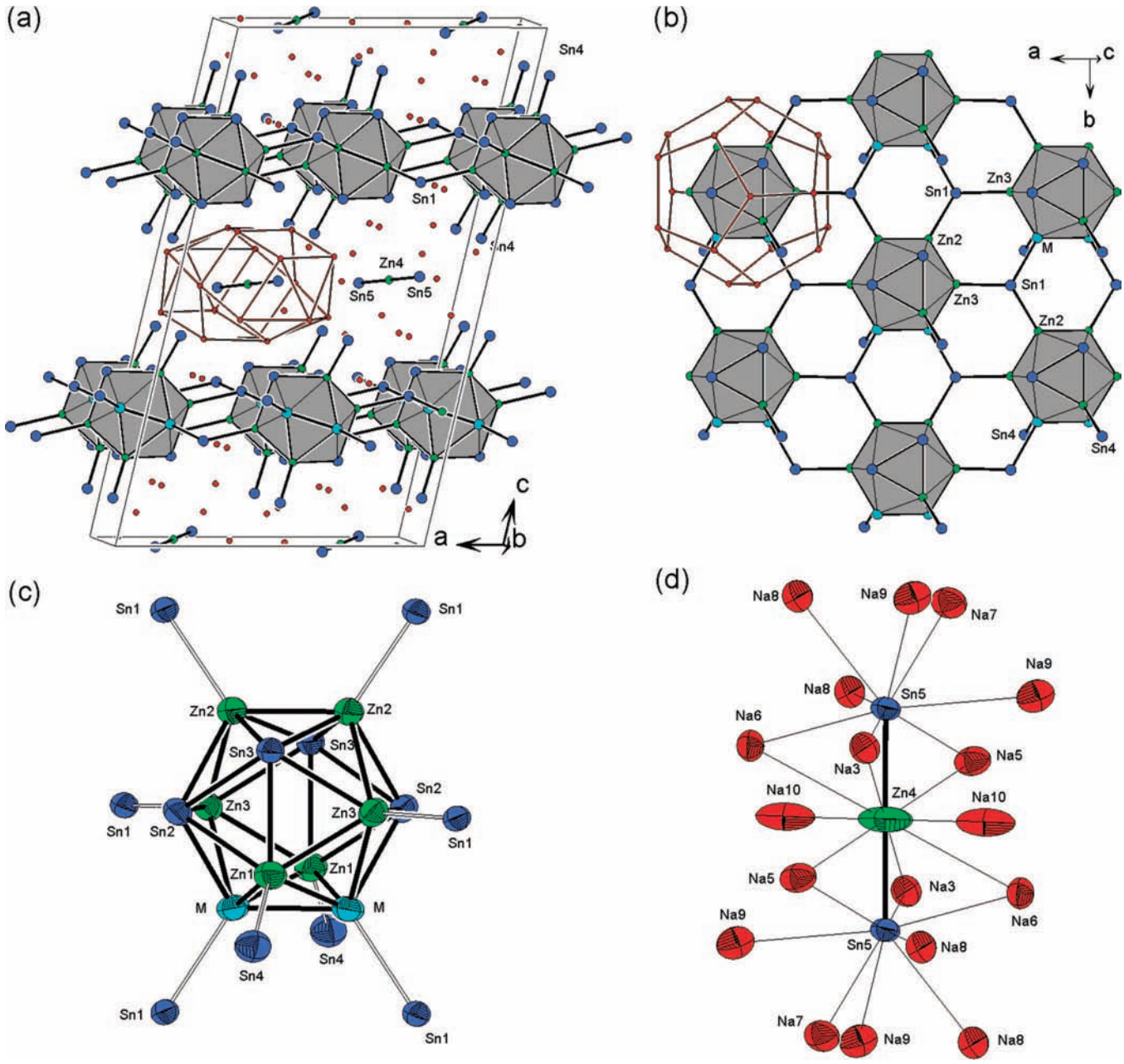

Figure 2. (a) Structural details of $Na_{20}Zn_8Sn_{11}$ (**3**): (a) Projection of the unit cell. (b) Perpendicular view on one layer of interconnected icosahedra; one $\{Na_{20}\}$ dodecahedron around an icosahedron is shown with red lines. (c) Anisotropic representation of the $\{Zn_7Sn_5\}$ icosahedron with *exo*-bonds (atoms are drawn at 90% probability level). (d) Arrangement of the Na atoms around the $\{ZnSn_2\}$ unit (atoms are drawn at 70% probability level). Na, Sn, Zn, and M = Zn/Sn atoms are represented as red, blue, green, and teal spheres, respectively.

]bis(dibenzoyl-methanato)-(Sn−Zn),[61] with d(Zn−Sn) = 2.58 and 2.63 Å, respectively, in which donor bonding from Sn to Zn(II) is assumed. Considering the high formal negative charge of $\{ZnSn_2\}^{6-}$, which generally increases interatomic distances, a multiple bond character must be assumed in the linear 16 valence-electron units.

Applying the extended Zintl−Klemm concept to $Na_{20}Zn_8Sn_{11}$ (**3**) and assuming the same $\{ZnSn_2\}^{6-}$ unit to be present with a PBO of 1.5, a total of 14 negative charges has to be distributed over the remaining atoms. Since the structure contains two $\{(3b)Sn1\}^-$ and two $\{(1b)Sn4\}^{3-}$ atoms, the remaining $\{Zn_7Sn_5\}$ icosahedra should carry a 6-fold negative charge. Treatment of the eight cluster *exo*-bonds as localized two-center-two-electron bonds leads to the following skeletal electron count for the icosahedron: Since an *exo*-bonded Zn_{exo} atom contributes one electron to the cluster unit, and an Sn_{exo} atom provides three electrons, the two M_{exo} atoms (50% Sn, 50% Zn) contribute two electrons on average. An additional Sn atom without an *exo*-bond provides two electrons to the cluster bonding. Hence, the $\{(Zn_{exo})_6(M_{exo})_2(Sn)_4\}$ icosahedron holds $(6 \times 1 + 2 \times 2 + 4 \times 2) = 18$ skeletal electrons. Assuming a *closo* cluster according to Wade's rules, the $\{Zn_7Sn_5\}$ icosahedron requires 26 skeletal electrons and therefore a formal charge of 8−. Thus, the cluster within the structure of $Na_{20}Zn_8Sn_{11}$ is lacking two electrons. One possibility to reach the electron count of an

(61) Jastrzebski, J. T. B. H.; Sypkens, H. A. J.; des Tombe, F. J. A.; van der Schaaf, P. A.; Boersma, J.; van Koten, G.; Spek, A. L.; Duisenberg, A. J. M. *J. Organomet. Chem.* **1990**, *396*, 25.

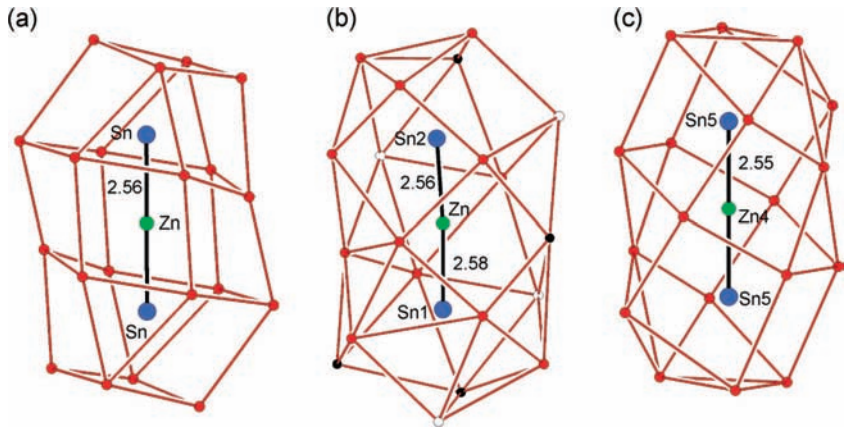

Figure 3. Alkali−metal polyhedra around the {$ZnSn_2$}$^{6-}$ unit in (a) (**1**), (b) (**2**), and (c) (**3**). The polyhedra consist of 20, 20, and 18 alkali atoms, respectively. Na, K, A = Na/K, Sn, and Zn atoms are represented as red, black, empty, blue, and green spheres, respectively.

Scheme 1. Possible Resonance Structures of {$ZnSn_2$}$^{6-}$ and Formal Oxidation States

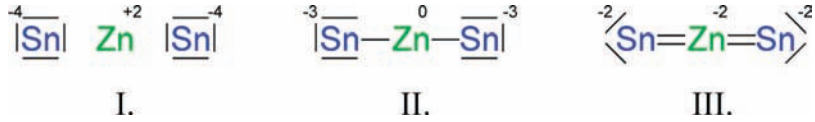

I. II. III.

Table 2. Calculated Values from NBO, AIM, and ELF Methods at the HF/3-21G- Level of Theory for {Sn−Zn−Sn}$^{6-}$ [a]

	Atomic charge		Zn−Sn bond	
	Zn	Sn	ρ	$\nabla^2\rho$
NBO_{solv}	+1.2	−3.6		
NBO_{Na20}	+0.8	−3.0		
AIM_{solv}	+1.0	−3.4	+0.042	+0.103
AIM_{Na20}	+0.3	−2.6	+0.042	+0.086
			Bond population	σ^2
ELF_{solv}			1.9	1.22
ELF_{Na20}			2.4	

[a] The electron density ρ and its Laplacian $\nabla^2\rho$ at the bond critical points obtained from the AIM method together with bond population and variance (σ^2) are listed.

electron-precise Zintl phase is that the mixed occupied site M is considered as fully occupied by Sn. Compound **3** however represents an electron-deficient compound which is not uncommon in complex structures and has been frequently reported for similar cluster phases.[62]

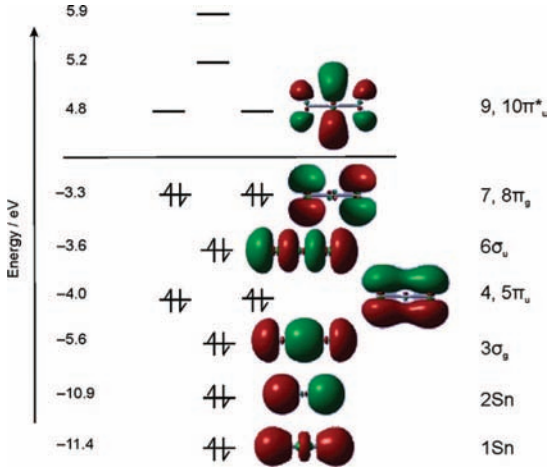

Figure 4. Molecular orbital diagram for the linear {$ZnSn_2$}$^{6-}{}_{solv}$ unit in Na_6ZnSn_2 (**1**).

3.3. Electronic Structure of Na_6ZnSn_2. 3.3.1. Structure Optimizations of the {$ZnSn_2$}$^{6-}$ unit were performed on the HF/3−21G level of theory using a polarizable continuum model (PCM) to ensure negative orbital energies of occupied orbitals. The calculations converged to a stable linear ground state with $D_{\infty h}$ symmetry and a bent transition state with C_s symmetry. The energy difference between the two conformations is ∼0.9 kcal/mol. The transition state of {$ZnSn_2$}$^{6-}$ has one negative frequency of −75.5962 cm^{-1}, a bond angle of 176.5035°, and Sn−Zn distances of 2.7927 and 2.8008 Å. The stable ground state displays a Sn−Zn distance of 2.7922 Å, which is significantly longer such as the ones found in the single crystal structure analyses (2.561(1) Å in **1**, 2.582(1) and 2.556(1) Å in **2**, and 2.546(1) Å in **3**). This discrepancy is due to the fact that the calculated value is the result of a gas phase calculation of a highly charged species using a PCM model and that counterions are not included. The ground-state geometry is encountered by starting from an almost linear structure (>179°), and the transition state structure is obtained with any bent structure as a starting model. Even the input of strongly bent units with a bond angle around 140° only led to the transition state mentioned above. The structure optimization of the {$ZnSn_2$}$^{6-}$ anion within a fixed {Na_{20}}$^{20+}$ cluster also leads to a bent transition state. We assume that the bending in **2** is the result of ionic interactions in the solid state. A structure optimization of the {$Na_{20}ZnSn_2$}$^{14+}$ unit was not considered due to the enormous calculation times required. For further interpretation of the results the experimental structure parameters for {$ZnSn_2$}$^{6-}$ and {Na_{20}}$^{20+}$ were used.

3.3.2. NBO, AIM, and ELF Analyses. The first approach of our calculations dealt with a PCM solvate model {$ZnSn_2$}$_{solv}$, and the second one with a {$ZnSn_2$}$_{Na20}$ model in which the anion is located in a {Na_{20}}$^{20+}$ cage. NBO, AIM, and ELF values have previously been calculated for charged molecules and led to quite reliable results.[63] The MO diagram calculated from the Gaussian wave function for {$ZnSn_2$}$^{6-}{}_{solv}$ confirms the relation-

(62) (a) Corbett, J. D. *Angew. Chem., Int. Ed.* **2000**, *39*, 670–690. (b) Belin, C.; Tillard-Charbonnel, M. *Prog. Solid St. Chem.* **1993**, *22*, 59, and references therein.

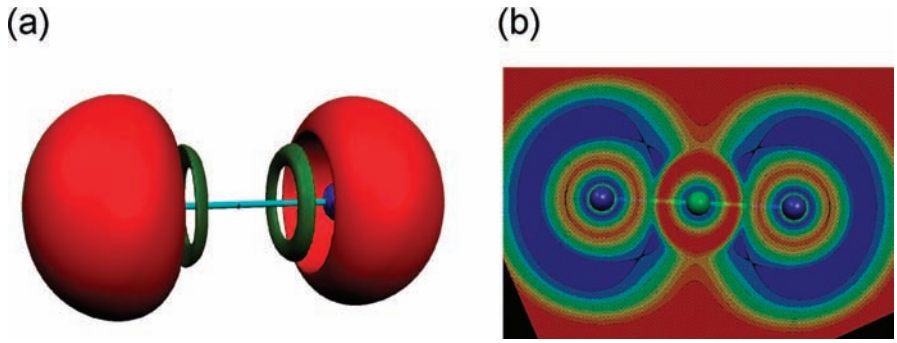

Figure 5. ELF calculations for $\{ZnSn_2\}^{6-}_{solv}$ in Na_6ZnSn_2 (**1**): (a) 3D-ELF isosurface of an all electron calculation (ELF = 0.78). (b) 2D-ELF contour diagram in a plane inclosing the anion.

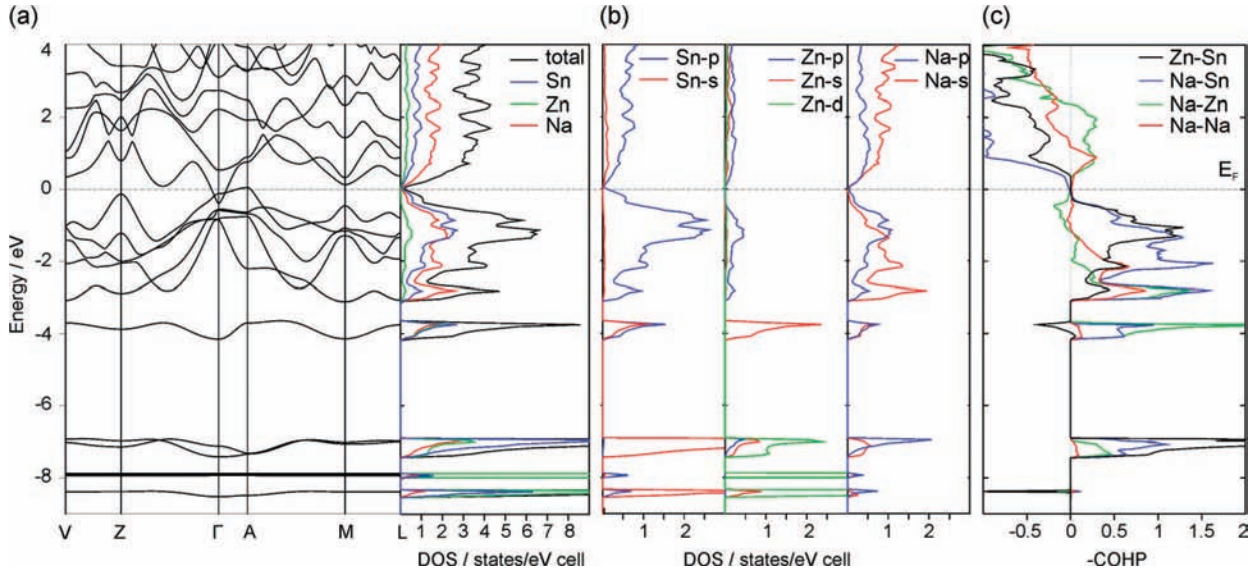

Figure 6. Results of the LMTO band structure calculation of Na_6ZnSn_2 (**1**). The Fermi level is set to 0 eV. (a) Band structure with projected total and partial density of states (DOS). (b) Separated contributions from the constituent elements. (c) Integrated-COHP diagram for the sum of all Zn−Sn (black), Na−Sn (blue), Na−Zn (green), and Na−Na (red) interactions as a function of energy.

ship to CO_2 and is shown in Figure 4. The corresponding diagram of the $\{ZnSn_2\}_{Na20}$ model is similar with considerably lower orbital energies due to the cation excess and is not shown. The eight low-lying molecular orbitals are occupied. The lowest two molecular orbitals are Sn-*s*/Sn-*s* bonding and nonbonding orbitals. The next higher MO which is formed by Zn-*s* and Sn-p_z orbitals (*z* direction along the interatomic vector) is consistent with the Zn−Sn σ bond. The three higher Zn-*p*/Sn-*p* orbitals are all bonding. A gap of ∼8.1 eV separates the HOMOs, the two degenerated nonbonding π_g orbitals, from the LUMOs, which originate from antibonding Zn-$p_{x,y}$/Sn-$p_{x,y}$ combinations.

To gain a better insight into the charge distribution within the 16 VE species according to Scheme 1, the anion was further investigated by NBO, AIM, and ELF calculations. A rather ionic nature of the $\{Sn-Zn-Sn\}^{6-}$ unit is evident from the calculated AIM and NBO charge distributions shown in Table 2. The NBO analysis places a larger negative charge on the two Sn atoms with comparable values for $\{ZnSn_2\}_{solv.}$ and $\{ZnSn_2\}_{Na20}$. The corresponding AIM values are smaller and are comparable with the NBO charges for the solvated model. The average NBO charge of Sn and Zn are −3.3 and +1.0, while the average AIM charges are −3 and +0.75, respectively. These values point toward a $\{(1b)Sn\}^{3-}$ anion and favor formulation II in Scheme 1.

The calculated low electron density together with its slightly positive Laplacian ($\nabla^2\rho$) at the Zn−Sn bond critical point indicates that the Zn−Sn interaction can be understood as a polarized covalent bonding. The ellipticity ϵ (a quantitative measure of the π character of the bond) is very small (0.015), indicating a cylindrical single or multiple bond. ELF calculations also reveal some contributions from covalent bonding. The torus-like localization domain around the Zn−Sn bond vector holds two electrons. Such an attractor shape usually reflects a multiple bonding situation like in ethyne.[65,66] Besides this the all-electron 3D-ELF (ELF value = 0.78) and the contour diagram in a plane including the C_∞ axis of the $\{ZnSn_2\}$ unit (Figure 5) show domains with high ELF values and the presence of lone pairs (monosynaptic valence basins) located at each Sn atom. The high variance of the domains indicates rather strong delocalization of electrons between the bonding domain and the lone pair.

3.3.3. Band Structure. Density of states (DOS) and crystal orbital Hamilton populations (COHP) calculations were carried out using the LMTO method to gain deeper insight into the nature of the cooperative bonding in the solid. The calculated total and projected DOS and −COHP plots for selected interactions, cumulated over all bonds per unit cell, are shown in Figure 6. Fat band representations of selected orbitals are

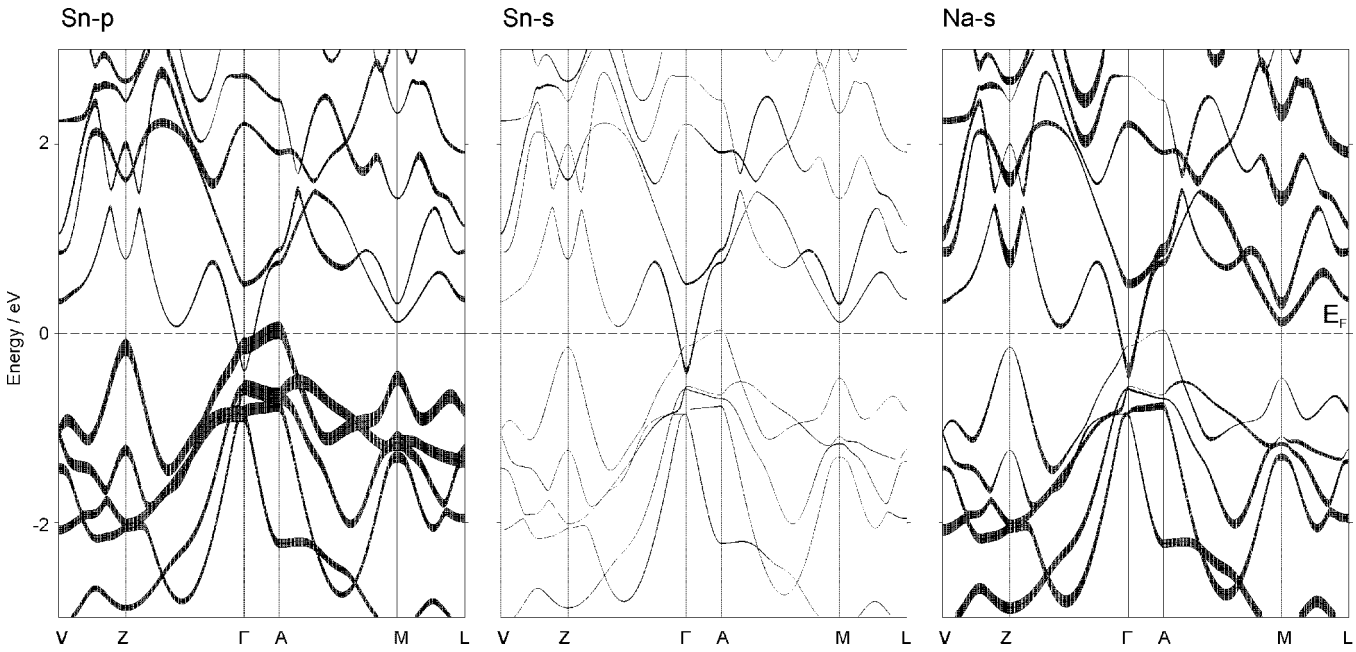

Figure 7. Fat band representation. The bands are drawn with a thickness representative of the orbital contributions of Sn-*p* (left), Sn-*s* (center), and Na-*s* (right) in Na_6ZnSn_2 (**1**).

given in Figure 7. The general shape of the band structure with bands having relatively small dispersions is consistent with the molecular (ionic) character of the compound as described above. The Zn-3*d* states are well localized and have core electron character: They are confined to a 2 eV range (−7 to −9 eV) and do not decisively interact with the *sp* bonding regions, and the −COHP plot (Figure 6c) in this energy section does not show the sharp Zn-*d* peaks which are present in the DOS projection of Figure 6b. The band at −7 eV shows mainly Sn-5*s* character with low contributions from Zn-3*d* and Na-3*p* states. At −4 eV a separated band emerges which has mainly Zn-4*s* character but also significant contributions from low-lying Sn-5*s*, Sn-5*p*, and Na-3*s* states. This orbital mixing indicates weak *sp* hybridization of Sn and antibonding interactions between Zn-*s* and Sn orbitals. This is in agreement with the molecular approach to the problem as worked out before (Figure 4).

The detached valence bands between −3.3 eV and the Fermi level mainly consist of Sn-5*p* states and contain some significant contributions from Na-3*s* and 3*p* orbitals (Figure 6b), which indicates an incomplete charge transfer to the anions. The apparent discrepancy to the fully ionic description of **1** underlines the formal character of the Zintl−Klemm concept, as charge transfer is not complete in a physical sense. Additionally, small, but noticeable, contributions of Zn-4*p* states are present. Therefore these bands represent mixing of the Zn-*p* orbitals with *p*-orbital-like lone pairs which are mainly located at the Sn atom. The Fermi level coincides with a low but nonzero DOS indicating an almost optimized electron count. Although band gaps are generally underestimated by LDA, the band structure reveals two bands crossing the Fermi level around the zone center. Fat band analyses (Figure 7 and Figure S3 in the Supporting Information) show that the intersecting valence band has mainly Sn-*p* and Na-*p* character, whereas the intersecting conduction band at Γ has mainly Na-*s* character with some Sn-*s* contribution. The metallic behavior originates from the alkali metals as it is known for alkali metal rich intermetallics such as Na_2In and K_5Bi_4.[63] The −COHP diagrams in Figure 6c reveal that the states below E_F have overall bonding character. The shoulder of the DOS with its maximum at ∼ −0.3 eV has no correspondent in the −COHP diagrams and is indicative of nonbonding states (lone pairs). The −COHP plots show all roughly optimized Na−Zn, Na−Sn, and Sn−Zn interactions. Na−Sn and Na−Zn interactions were considered up to 4 Å and have averaged −ICOHP values of 0.12 and 0.32 eV per contact (Table S4, Supporting Information). The average Na−Na interaction with 0.07 eV is considerably weaker, and altogether these contacts are significantly weaker than the Zn−Sn overall bonding energy of 2.74 eV.

4. Summary and Conclusions

The linear unit $\{ZnSn_2\}$ has been found in the crystal structures of the three new intermetallic compounds Na_6ZnSn_2 (**1**), $Na_{4.24}K_{1.76(1)}ZnSn_2$ (**2**), and $Na_{20}Zn_8Sn_{11}$ (**3**). The $\{ZnSn_2\}^{6-}$ anion is a new representative of a 16 VE species, and the bonding within this unit can be readily explained with the $(8-N)$ rule for **1** and **2**. Na_6ZnSn_2 exhibits a weak diamagnetism as shown by negative susceptibility values during temperature-dependent magnetic measurements. The structure of $Na_{20}Zn_8Sn_{11}$ contains further polyhedral motifs typical of electron-deficient structures.[67] ELF calculations indicate a rather covalent nature of the Sn−Zn interaction in the linear $\{ZnSn_2\}^{6-}$ anion with multiple-bond character. This is in agreement with LMTO band structure calculations, which reveal significant Zn-*s* and -*p* with Sn-*s* and -*p* orbital mixing below E_F. Furthermore, the band

(63) (a) Li, B.; Corbett, J. D. *Inorg. Chem.* **2006**, *45*, 2960. (b) Gascoin, F.; Sevov, S. C. *Inorg. Chem.* **2001**, *40*, 5177.
(64) (a) Sambrano, J. R.; Gracia, L.; Andre's, J.; Berski, S.; Beltra'n, A. *J. Phys. Chem. A* **2004**, *108*, 10850. (b) Quiñonero, D.; Frontera, A.; Deyà, P. M.; Alkorta, I.; Elguero, J. *Chem. Phys. Lett.* **2008**, *460*, 406.
(65) Savin, A.; Nesper, R.; Wengert, S.; Fässler, T. F. *Angew. Chem.* **1997**, *109*, 1892.
(66) Kohout, M.; Wagner, F. R.; Grin, Y. *Theor. Chem. Acc.* **2002**, *108*, 150.
(67) Mao, J. G.; Goodey, J.; Guloy, A. M. *Inorg. Chem.* **2004**, *43*, 282.

structure calculations show that the alkali metals are significantly involved in the chemical bonding of the anion and that they are also responsible for a nonzero DOS at E_F. AIM and NBO analyses rather point toward a twofold single-bonded central Zn atom. The results are consistent with the so-called double bond rule[68] which states that elements outside the first row of the periodic table have a much lower tendency to form multiple bonds.[69]

Acknowledgment. We thank Dr. B. Wahl for discussions of the crystal structure solutions, Dr. S. D. Hoffmann for magnetic measurements, Dipl.-Chem. S. Baer for supporting laboratory work, and Dr. A. Schier for revision of the manuscript.

Supporting Information Available: Anisotropic displacement parameters (/Å^2) and interatomic distances ($\leq$4 Å) for Na_6ZnSn_2, $Na_{4.24}K_{1.76(1)}ZnSn_2$, and $Na_{20}Zn_8Sn_{11}$. ICOHP values for selected interatomic contacts in Na_6ZnSn_2. More detailed figures of the solid state structures. Fat band plots of Zn-*p* and Na-*p* for Na_6ZnSn_2. Magnetic susceptibility versus temperature plots for Na_6ZnSn_2. X-ray crystallographic files in CIF format. Complete ref 38. This material is available free of charge via the Internet at http://pubs.acs.org.

JA806737K

(68) (a) Mulliken, R. S. *J. Am. Chem. Soc.* **1955**, *77*, 884. (b) Pitzer, K. S. *J. Am. Chem. Soc.* **1948**, *70*, 2140. (c) Power, P. P. *Chem. Rev.* **1999**, *99*, 3463.
(69) Bouhadir, G.; Bourissou, D. *Chem. Soc. Rev.* **2004**, *33*, 210.